

Dynamics of coupled Kuramoto oscillators with distributed delays

Cite as: Chaos 31, 103107 (2021); doi: 10.1063/5.0055467

Submitted: 29 April 2021 · Accepted: 7 September 2021 ·

Published Online: 4 October 2021





View Online



Export Citation



CrossMark

A. Ross,¹ S. N. Kyrychko,²  K. B. Blyuss,¹  and Y. N. Kyrychko^{1,a)} 

AFFILIATIONS

¹Department of Mathematics, University of Sussex, Falmer, Brighton BN1 9QH, United Kingdom

²Polyakov Institute of Geotechnical Mechanics, National Academy of Sciences of Ukraine, Simferopolska str. 2a, Dnipro 49005, Ukraine

Note: This paper is part of the Focus Issue, In Memory of Vadim S. Anishchenko: Statistical Physics and Nonlinear Dynamics of Complex Systems.

a) Author to whom correspondence should be addressed: y.kyrychko@sussex.ac.uk

ABSTRACT

This paper studies the effects of two different types of distributed-delay coupling in the system of two mutually coupled Kuramoto oscillators: one where the delay distribution is considered inside the coupling function and the other where the distribution enters outside the coupling function. In both cases, the existence and stability of phase-locked solutions is analyzed for uniform and gamma distribution kernels. The results show that while having the distribution inside the coupling function only changes parameter regions where phase-locked solutions exist, when the distribution is taken outside the coupling function, it affects both the existence, as well as stability properties of in- and anti-phase states. For both distribution types, various branches of phase-locked solutions are computed, and regions of their stability are identified for uniform, weak, and strong gamma distributions.

Published under an exclusive license by AIP Publishing. <https://doi.org/10.1063/5.0055467>

Many real-life systems can be effectively modeled as coupled networks, and the dynamical behavior of the overall system depends on intrinsic parameters of the nodes and connections between them. Interactions between nodes are usually delayed due to, for example, propagation time of the signal or processing times, and these time delays play an important role in determining dynamics of such systems. In this paper, we study the simplest motif of two coupled elements to explore the diversity of the dynamics and to concentrate on the role played by the time delays, which can then be used in the analysis of larger networks. Since in many realistic settings, the delays are not constant, we assume that the time delays follow some delay distribution and consider a system of two coupled Kuramoto oscillators with two different ways of how delay distribution is included in the coupling. Our results show how the dynamics of phase-locked solutions depends not only on the type of the distribution kernel, but also on how it arises in the model.

I. INTRODUCTION

Systems of coupled oscillators have been widely used to describe a variety of phenomena in different scientific fields,

ranging from brain activity behavior to network modeling.¹⁻⁷ Research in this field facilitates the development of understanding of how groups of moving objects, such as murmuration of starlings, flocks of fireflies, crowds of people, or collections of autonomous robots can reach a consensus and move in formation without centralized coordination.⁸⁻¹¹ Synchronization in complex systems occurs when the behavior of individual nodes in the network adjusts to a common time evolution. In 1967, Winfree proposed that large systems of interacting oscillators can be used to model many rhythmic processes in biology.¹² He found that organized collective behavior and formation of patterns are possible, even when there are differences between oscillators, and he proposed a mathematical formulation of synchronized behavior. Inspired by Winfree's work, in 1975, Kuramoto proposed a tractable model for oscillator synchronization, which has become one of the most representative models of coupled phase oscillators.¹³ Synchronized behavior has been subsequently analyzed for various network topologies, including adaptive, small scale, and weighted networks.¹⁴⁻¹⁷ Besides complete synchronization, various other types of partially synchronized dynamics, such as chimera states,¹⁸⁻²⁰ remote or relay synchronization,^{21,22} and cluster synchronization^{23,24} have been studied.

Besides traditional applications of coupled oscillators in engineering, physics, and biology, recently, synchronization of coupled oscillators has been used to develop models of financial market behavior and business cycle fluctuations. Groth and Ghil²⁵ studied dynamical properties of business cycle fluctuations by applying the methodology of multivariate singular spectrum analysis to identify oscillator modes and to investigate whether the modes are shared by clusters of phase- and frequency-locked oscillators. Ikeda *et al.*²⁶ analyzed gross domestic product time series to find entrainment and partial phase locking to be a direct evidence of synchronization in business cycles. Synchronization in this context is explained by developing a coupled limit-cycle oscillator model, where the interaction due to international trade is interpreted as the origin of the synchronization.

Coupling, delay, and topology are the three main factors characterizing interactions in systems of coupled oscillators.^{27,28} Information exchange between different elements in the system involves the propagation of a signal with a finite speed, causing a communication delay.^{27,29} Time delays can be considered discrete or distributed with some distribution kernel.³⁰ Discrete delays in the coupling of coupled phase oscillators also contribute to effects such as multistability, amplitude, and oscillation death.^{31–35} In real world applications, the processing delay rarely has the same length at every time step but instead follows a distribution with some mean value.^{36,37}

Systems of almost identical oscillators that are weakly coupled are commonly modeled as Kuramoto oscillators, which assumes that each oscillator has its own natural frequency, and information exchange between the oscillators is sinusoidally related to the phase difference between the oscillators. A phase-locked solution occurs when all oscillators are completely synchronized; the oscillators share the same frequency, and each cycle of oscillations starts at the same time.⁸

The effects of distributed time delays in the context of coupled oscillators have been studied on the example of coupled Stuart–Landau oscillators,^{38,39} where it was shown that larger widths of delay distribution increase the regions of amplitude death in terms of average frequency, frequency detuning, and parameters of the coupling, such as coupling strength and phase. This work also explored the influence of mean time delay and the width of delay distribution on the existence and stability of various branches of phase-locked solutions. Using a globally coupled network of oscillators, it was subsequently found that increasing the width of the uniform distribution for the same mean delay allows aging transition to happen for a smaller coupling strength and a smaller proportion of inactive elements.^{40,41} Synchronization of network oscillators can also be analyzed using the framework of a master stability function.^{42–44} The master stability function approach has later been extended to systems of Stuart–Landau oscillators, and it was shown how the stability of synchronized solutions in networks with distributed delay coupling can be determined through a semi-analytic computation of the corresponding Floquet exponents.⁴⁵

In this paper, we consider the effect of distributed-delay coupling in a system of two mutually coupled Kuramoto oscillators. In particular, we are interested in understanding if and how various distributions of the time-delayed kernel influence the dynamics of the system, including the existence and stability of phase-locked

solutions. Unlike the case of the discrete time delays, here, the distribution in the coupling can arise either inside or outside the coupling function. Motivation for analyzing this problem comes from many real-world applications such as synchronization in wireless sensor networks^{46,47} and smart/power grids.^{3,48} Such system with discrete delay coupling was first analyzed by Schuster and Wagner,⁴⁹ and it has the form

$$\begin{aligned}\dot{\theta}_1(t) &= \omega_1 + \kappa \sin(\theta_2(t - \tau) - \theta_1(t)), \\ \dot{\theta}_2(t) &= \omega_2 + \kappa \sin(\theta_1(t - \tau) - \theta_2(t)),\end{aligned}\quad (1)$$

where $\theta_{1,2}$ are phases of the oscillators, ω_1, ω_2 are natural frequencies, κ is the coupling strength, and it is assumed that oscillators interact with a discrete time delay τ . The authors have shown that unlike the case without time delays in the connection, this system exhibits a range of synchronized solutions. This work was later extended by D’Huys *et al.* to the case of identical mutually coupled oscillators to study the interplay of various network motifs, symmetry, and time delays.⁵⁰ It was shown that the time delays have different effects depending on the type of symmetry in the system, and that for some network configurations, it is possible to maintain zero-lag synchronization even for large values of time delays in the coupling.

In Sec. II, we introduce the system of Kuramoto oscillators with a general distributed-delay connection, where the distribution is taken inside the coupling function. We analytically derive the general characteristic equations for in-phase and anti-phase solutions and look at two commonly used in the literature distribution kernels, namely, uniform and gamma distributions. Numerical simulations are performed to identify the regions of stable in- and anti-phase solutions for various parameter values. Section III is devoted to the analysis of two mutually coupled Kuramoto oscillators, where the distributed-delay coupling is considered outside the coupling function. Analytical calculations and numerical simulations show how different distribution kernels influence the stability of in- and anti-phase solutions. This paper concludes with the summary of results and potential further work.

II. DELAY DISTRIBUTION INSIDE THE COUPLING FUNCTION

Since we are interested in the role of distribution of time delays in synchronization properties of two identical mutually coupled Kuramoto oscillators, we consider the system (1) with $\omega_1 = \omega_2 = \omega_0$, which can be rescaled using $\hat{\kappa} = \kappa/\omega_0$, $\hat{\tau} = \omega_0\tau$, and $\hat{t} = \omega_0 t$ to become

$$\begin{aligned}\dot{\theta}_1(t) &= 1 + \kappa \sin \left[\int_0^\infty g(s)\theta_2(t-s)ds - \theta_1(t) \right], \\ \dot{\theta}_2(t) &= 1 + \kappa \sin \left[\int_0^\infty g(s)\theta_1(t-s)ds - \theta_2(t) \right],\end{aligned}\quad (2)$$

where θ_1, θ_2 are the phases of the oscillators, κ is the coupling strength, and the hats have been omitted. The kernel of the delay distribution $g(\cdot)$ is assumed to be positive-definite and normalized to unity,

$$g(s) \geq 0 \quad \text{and} \quad \int_0^\infty g(s)ds = 1.$$

If the delay distribution is governed by the Dirac delta function $g(u) = \delta(u)$, the two oscillators in system (2) are interacting instantaneously, reducing it to the Adler equation,⁵¹ and if $g(u) = \delta(u - \tau)$, then the system (2) reduces to the case of discrete time-delayed coupling between oscillators considered in Ref. 50.

Phase-locked solutions are states that are characterized by a collective frequency ω , with which all oscillators evolve in time, and a certain constant phase. Looking for solutions in the form $\theta_1 = \omega t + c$, $\theta_2 = \omega t$, where c is an unknown constant, shows that the only possible values of c are $c = 0$ and $c = \pi$. The case of $c = 0$ corresponds to the in-phase oscillators, and $c = \pi$ describes the anti-phase oscillators. The coupling is attractive when the coupling strength κ is positive; therefore, the oscillators progress toward a symmetric, in-phase state, whereas the coupling is repulsive when the coupling strength κ is negative; therefore, the oscillators move toward an anti-phase behavior. Due to the symmetry of the coupling function, stable in-phase and anti-phase solutions interchange when the coupling strength κ changes from positive to negative and vice versa. Delayed coupling can induce multiple solutions with different locking frequencies in the frequency-locked symmetric and antisymmetric states.

Besides in-phase and anti-phase solutions, it is possible to find the solutions with $\omega = \pi/(2\tau_m) \pm n\pi$, $n = 0, 1, 2, \dots$, which is a degenerate case, and such solutions will only exist for $\tau_m \geq \pi/(2(1 + |\kappa|))$, where τ_m is the mean time delay. However, since the frequency of these solutions does not depend on the coupling strength and it is not possible to reduce the delayed model to the case of instantaneous coupling by taking $\tau_m \rightarrow 0$, we are not considering those solutions in this paper.

For the in-phase solutions, the phases satisfy $\theta_1(t) = \theta_2(t) = \omega t$, with frequency ω that obeys the following equation:

$$\omega = 1 - \kappa \sin \left[\omega \int_0^\infty sg(s) ds \right]. \tag{3}$$

Similarly, for the anti-phase solutions with $\theta_1(t) = \theta_2(t) + \pi = \omega t$, the system of equations reduces to the equation

$$\omega = 1 + \kappa \sin \left[\omega \int_0^\infty sg(s) ds \right]. \tag{4}$$

Both equations are only dependent on the mean of the delay distribution $g(s)$, and neither the shape of the distribution $g(s)$ nor the number of oscillators in the system affects this equation for the collective frequency.

Linearizing the system (2) near the in-phase/anti-phase solutions gives the following characteristic equation:

$$\left[\lambda \pm \kappa \cos \left(\omega \int_0^\infty sg(s) ds \right) \right]^2 - \kappa^2 \cos^2 \left[\omega \int_0^\infty sg(s) ds \right] [\mathcal{L}g(\lambda)]^2 = 0, \tag{5}$$

where $\{\mathcal{L}g\}(\lambda) = \int_0^\infty g(s)e^{-\lambda s} ds$ is the Laplace transform of the function $g(s)$ and \pm corresponds to the in-phase/anti-phase solutions, respectively.

A. Uniform delay distribution

In order to make further analytical progress, we consider a uniformly distributed delay kernel given by

$$g(s) = \begin{cases} \frac{1}{2\rho} & \text{when } \tau - \rho \leq s \leq \tau + \rho, \\ 0 & \text{otherwise,} \end{cases} \tag{6}$$

where τ is the mean time delay and 2ρ is the width of the distribution. The characteristic equation (5) now becomes

$$\lambda \pm |\kappa| \cos(\omega\tau) = \pm |\kappa| \cos(\omega\tau) [\mathcal{L}g(\lambda)], \tag{7}$$

where

$$[\mathcal{L}g(\lambda)] = e^{-\lambda\tau} \frac{\sinh(\lambda\rho)}{\lambda\rho},$$

and the eigenvalues λ determine the stability of the solutions. For any values of τ and ρ , one of the roots of this equation is $\lambda = 0$, which corresponds to an arbitrary phase shift in the phase-locked solutions. In order to explore whether stability of solutions can change through a Hopf bifurcation, we look for solutions of the characteristic equation (7) in the form $\lambda = i\Omega$, $\Omega > 0$. Separating real and imaginary parts gives

$$\begin{aligned} \pm a &= \pm a \cos \Omega\tau \frac{\sin \Omega\rho}{\Omega\rho}, \\ \Omega &= \mp a \sin \Omega\tau \frac{\sin \Omega\rho}{\Omega\rho}, \end{aligned}$$

where $a = |\kappa| \cos(\omega\tau)$. Squaring and adding these equations yields

$$\Omega^2 + a^2 = a^2 \left(\frac{\sin \Omega\rho}{\Omega\rho} \right)^2.$$

Since $|\sin \Omega\rho / \Omega\rho| \leq 1$, this equation has no solutions for $\Omega > 0$. This means that there is no possibility for phase-locked solutions to lose/gain their stability via a Hopf bifurcation. Hence, any stability change in this case can only occur through a steady-state bifurcation.

In order to identify regions of stability for in-phase and anti-phase solutions, we rewrite the linearized system with the uniformly distributed kernel as

$$\dot{\phi}(t) = L_0\phi(t) + \frac{1}{2\rho} \int_{-(\tau+\rho)}^{-(\tau-\rho)} M\phi(t+s) ds, \tag{8}$$

where $\phi = (\phi_1, \phi_2)$, $\theta_1(t) = \omega t + \epsilon\phi_1(t)$, $\theta_2(t) = \omega t + \epsilon\phi_2(t)$ (in-phase) and $\theta_2(t) = \omega t - \pi + \epsilon\phi_2(t)$ (anti-phase), $0 < \epsilon \ll 1$, and

$$\begin{aligned} L_0 &= \begin{pmatrix} \mp\kappa \cos(\omega\tau) & 0 \\ 0 & \mp\kappa \cos(\omega\tau) \end{pmatrix}, \\ M &= \begin{pmatrix} 0 & \pm\kappa \cos(\omega\tau) \\ \pm\kappa \cos(\omega\tau) & 0 \end{pmatrix} \end{aligned}$$

for the in-phase/anti-phase locked solutions, respectively (a detailed derivation of this equation is shown in the Appendix). System (8) is now in the form suitable for computing the maximum real part of the eigenvalues using the algorithm described in Breda *et al.*⁵² and implemented in traceDDE suite in Matlab.

Figure 1 shows the stability of the in-phase and anti-phase solutions as a function of the time delay τ and the coupling strength

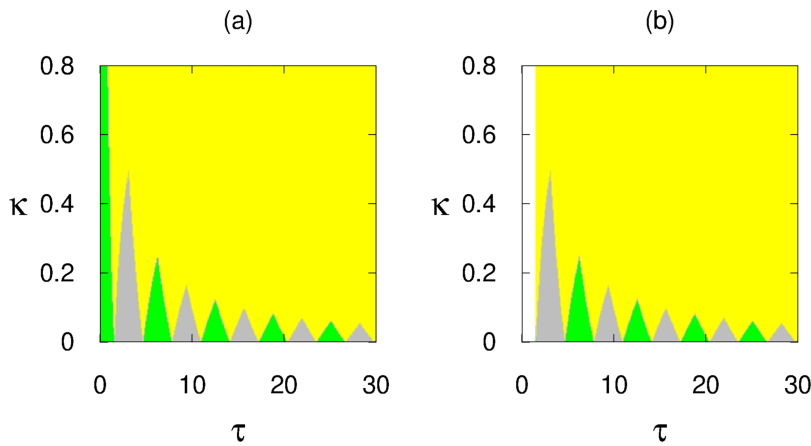


FIG. 1. Stability regions of phase-locked solutions of system (2) for a uniform delay distribution (6): green regions correspond to stable in-phase solutions only, gray regions correspond to stable anti-phase solutions only, and yellow indicates the region where both types of phase-locked solutions coexist and are stable. (a) $\rho = 0.0001$ and (b) $\rho = 1.5$.

κ for different values of the width of the uniform distribution ρ . For small values of the coupling strength κ , the system alternates between stable in-phase and anti-phase states, and increasing the coupling strength allows for both solutions to co-exist. Increasing the mean time delay leads to the shrinking of the stability islands, while increase in the distribution width ρ does not play a role in the overall stability structure unlike the cases considered in Refs. 39 and 41, though it bounds from below the smallest mean time delay, for which the phase-locked solutions can be observed.

In Figs. 2 and 3, we are illustrating branches of stable and unstable in- and anti-phase solutions as functions of locking frequencies ω and the coupling strength κ or the mean time delay τ for a fixed width of the distribution ρ . These figures show that increasing the mean time delay leads to a faster switching between different branches (i.e., a higher number of branches within the same range of possible phase-locked frequencies), whereas higher values of the coupling strength κ and the mean time delay τ enhance

multistability. The width of the delay distribution ρ does not affect either the number of branches or their stability.

B. Weak and strong gamma distributions

The second example we consider is the gamma distribution kernel with an integer shape (or order parameter) p and scale parameter γ , which has the form

$$g_\gamma^p(s) = \frac{s^{p-1} \gamma^p e^{-\gamma s}}{(p-1)!}, \tag{9}$$

where $\gamma, p \geq 0$. With this delay distribution kernel, the characteristic equation (5) transforms into

$$\left[\lambda \pm \kappa \cos\left(\frac{\omega p}{\gamma}\right) \right]^2 - \kappa^2 \cos^2\left(\frac{\omega p}{\gamma}\right) \left[\frac{\gamma^p}{(\lambda + \gamma)^p} \right]^2 = 0, \tag{10}$$

where \pm corresponds to the in-phase/anti-phase solutions. The delay kernel with gamma distribution of order $p = 1$ is known as

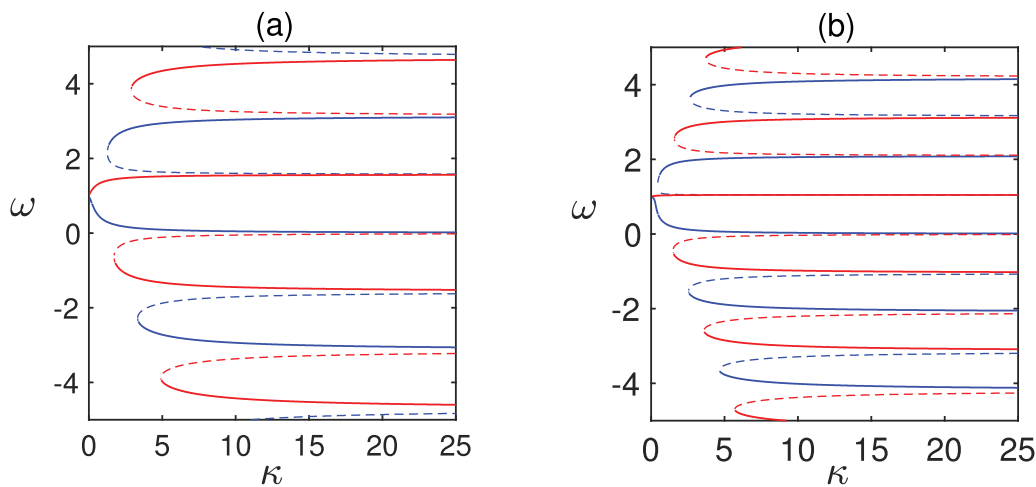


FIG. 2. Branches of phase-locked solutions of system (2) with a uniform distribution (6) for different mean time delays and the same width of the distribution $\rho = 0.5$. Solid lines denote stable branches, and dashed lines denote unstable branches. Blue indicates in-phase solutions and red anti-phase solutions. (a) $\tau = 2$. (b) $\tau = 3$.

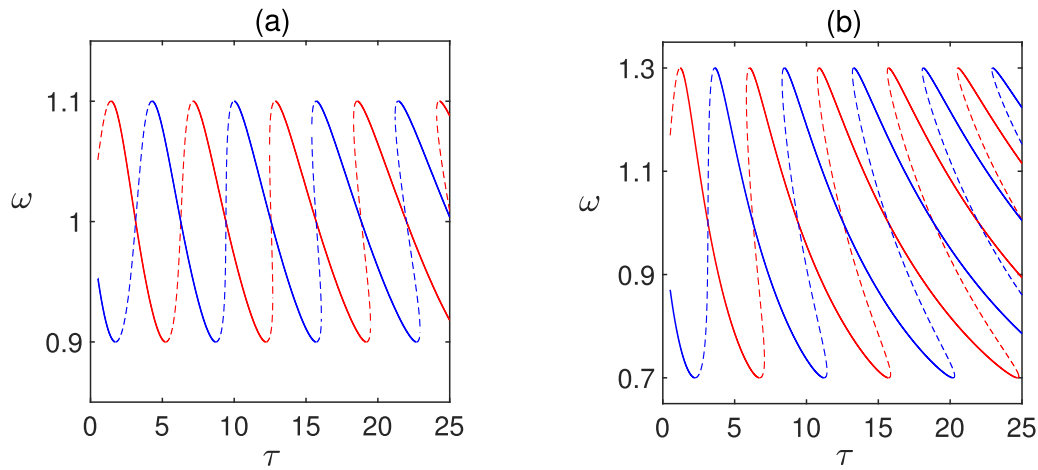


FIG. 3. Branches of phase locked solutions of system (2) with a uniform distribution (6) for different coupling strengths κ and the same width of the distribution $\rho = 0.5$. Solid lines denote stable branches, and dashed lines denote unstable branches. Blue indicates in-phase solutions and red anti-phase solutions. (a) $\kappa = 0.1$. (b) $\kappa = 0.3$.

the weak kernel and has an exponential form; i.e., $g(s) = \gamma e^{-\gamma s}$. We use the linear chain trick described in Ref. 53 to convert the system with a gamma distributed delay into a system of ODEs.

Introducing new variables

$$\begin{aligned} \phi_3(t) &= \int_0^\infty \gamma e^{-\gamma s} \phi_2(t-s) ds, \\ \phi_4(t) &= \int_0^\infty \gamma e^{-\gamma s} \phi_1(t-s) ds, \end{aligned}$$

we obtain

$$\begin{aligned} \dot{\phi}_1(t) &= \pm \kappa \cos\left(\frac{\omega}{\gamma}\right) \phi_3(t) \mp \kappa \cos\left(\frac{\omega}{\gamma}\right) \phi_1(t), \\ \dot{\phi}_2(t) &= \pm \kappa \cos\left(\frac{\omega}{\gamma}\right) \phi_4(t) \mp \kappa \cos\left(\frac{\omega}{\gamma}\right) \phi_2(t), \\ \dot{\phi}_3(t) &= -\gamma \phi_3(t) + \gamma \phi_2(t), \\ \dot{\phi}_4(t) &= -\gamma \phi_4(t) + \gamma \phi_1(t) \end{aligned}$$

for in-phase/anti-phase dynamics, respectively. Using this system, we find that the characteristic equation for the in-phase/anti-phase solutions has the form

$$\left[\lambda \pm \kappa \cos\left(\frac{\omega}{\gamma}\right) \right]^2 - \kappa^2 \cos^2\left(\frac{\omega}{\gamma}\right) \left[\frac{\gamma}{\lambda + \gamma} \right]^2 = 0, \quad (11)$$

and the eigenvalues are $\lambda_1 = 0$, $\lambda_2 = -\gamma \mp \kappa \cos\left(\frac{\omega}{\gamma}\right)$, and

$$\lambda^2 + \lambda \left[\gamma \pm \kappa \cos\left(\frac{\omega}{\gamma}\right) \right] \pm 2\gamma\kappa \cos\left(\frac{\omega}{\gamma}\right) = 0, \quad (12)$$

which yields the stability condition as $\kappa \cos(\omega\tau_m) > 0$ for the in-phase solution and $\kappa \cos(\omega\tau_m) < 0$ for the anti-phase solution, where the mean time delay τ_m is expressed as $\tau_m = 1/\gamma$.

Smaller values of γ (a large value of τ_m) with sufficiently small coupling strength κ induce multiple switches between stable in-phase and anti-phase solutions, and the size of the parameter regions, where only one type of solutions is stable, grows with increasing γ . Increasing the coupling strength leads to simultaneous stabilization of multiple branches and the resulting multistability, as shown in Fig. 4. Figure 5 illustrates that by increasing the value of γ , which corresponds to a reduction in the mean time delay, in-phase and anti-phase states alternate, but the number of possible

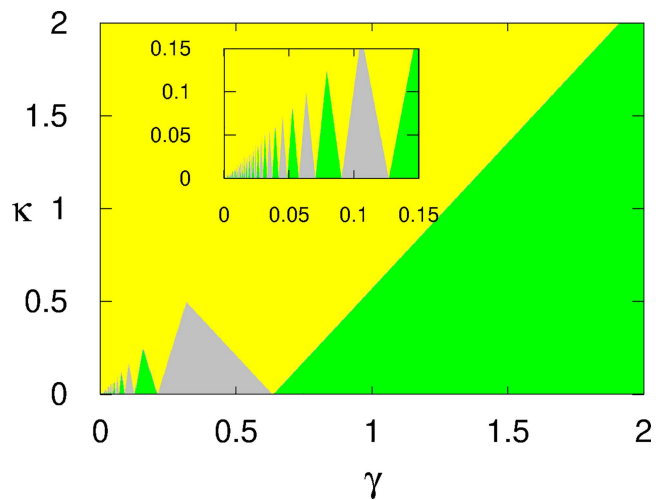


FIG. 4. Stability regions of phase-locked solutions of system (2) with a weak ($p = 1$) gamma distribution (9): green regions correspond to stable in-phase solutions only, gray regions correspond to stable anti-phase solutions only, and yellow indicates the region where both types of phase-locked solutions coexist and are stable.

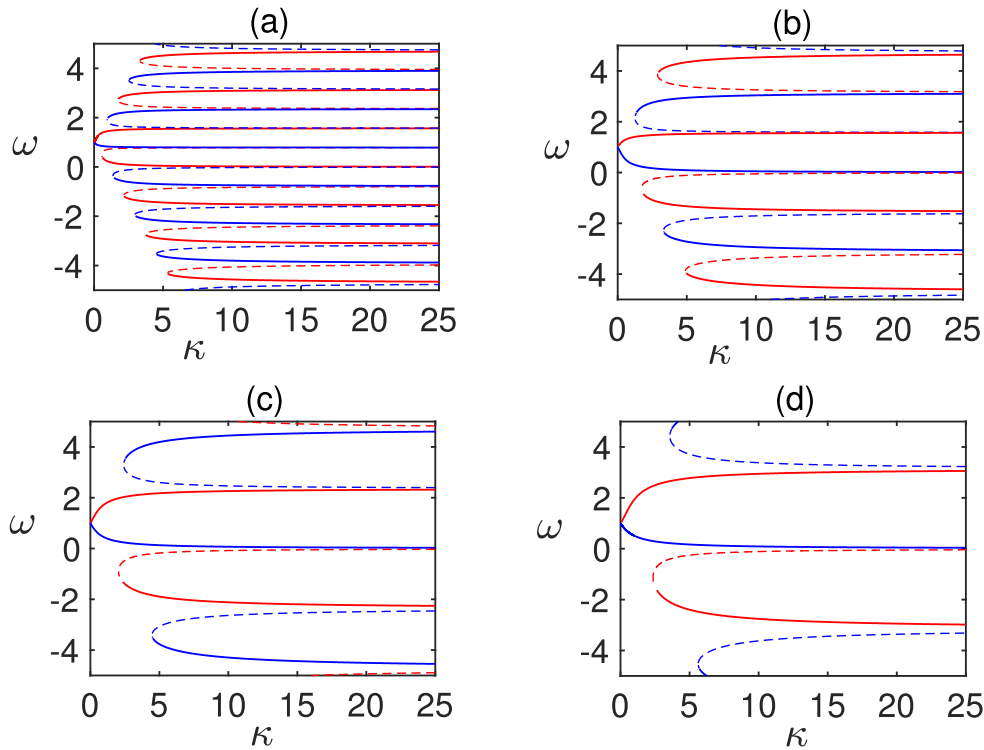


FIG. 5. Branches of phase locked solutions of (2) with a weak ($p = 1$) gamma distribution (9). Solid lines denote stable branches, and dashed lines denote unstable branches. Blue indicates in-phase solutions and red anti-phase solutions. (a) $\gamma = 0.25$, (b) $\gamma = 0.5$, (c) $\gamma = 0.75$, and (d) $\gamma = 1$.

multistable solutions decreases, and phase-locked solutions only appear starting with larger values of the coupling strength.

We now consider the gamma distribution of order $p = 2$, referred to as the strong delay kernel, where we have $g(s) = \gamma^2 s e^{-\gamma s}$. Similarly to the weak delay kernel, we can re-write the system in the following form:

$$\begin{aligned}
 \dot{\phi}_1(t) &= \pm \kappa \cos\left(\frac{2\omega}{\gamma}\right) \phi_4(t) \mp \kappa \cos\left(\frac{2\omega}{\gamma}\right) \phi_1(t), \\
 \dot{\phi}_2(t) &= \pm \kappa \cos\left(\frac{2\omega}{\gamma}\right) \phi_6(t) \mp \kappa \cos\left(\frac{2\omega}{\gamma}\right) \phi_2(t), \\
 \dot{\phi}_3(t) &= -\gamma \phi_3(t) + \gamma \phi_2(t), \\
 \dot{\phi}_4(t) &= -\gamma \phi_4(t) + \gamma \phi_3(t), \\
 \dot{\phi}_5(t) &= -\gamma \phi_5(t) + \gamma \phi_1(t), \\
 \dot{\phi}_6(t) &= -\gamma \phi_6(t) + \gamma \phi_5(t).
 \end{aligned}
 \tag{13}$$

The eigenvalues of the characteristic equation for the system (13) are $\lambda_1 = 0$, $\lambda_2 = -\gamma \mp \kappa \cos\left(\frac{2\omega}{\gamma}\right)$ (both of multiplicity two), and

$$\lambda^2 + \lambda \left[\gamma \pm \kappa \cos\left(\frac{2\omega}{\gamma}\right) \right] \pm 2\gamma \kappa \cos\left(\frac{2\omega}{\gamma}\right) = 0, \tag{14}$$

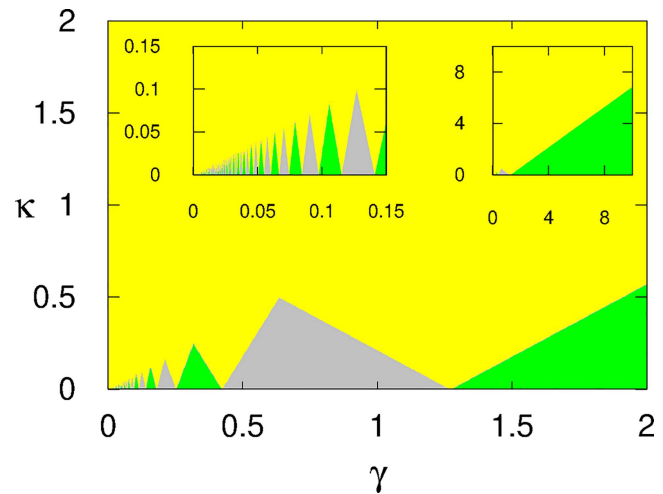


FIG. 6. Stability regions of phase-locked solutions of system (2) with a strong ($p = 2$) gamma distribution (9): green regions correspond to stable in-phase solutions only, gray regions correspond to stable anti-phase solutions only, and yellow indicates the region where both types of phase-locked solutions coexist and are stable.

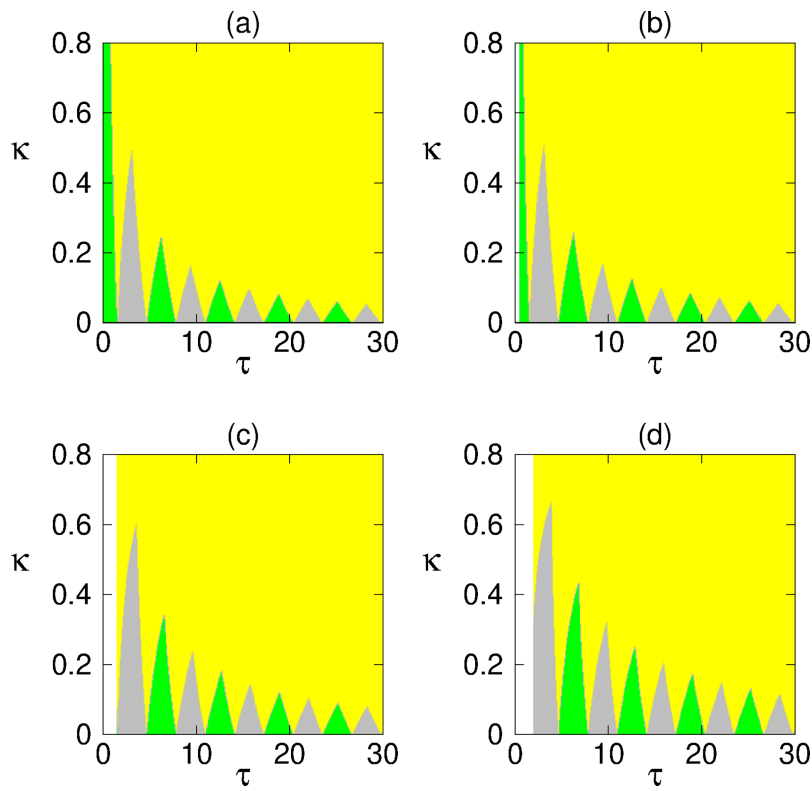


FIG. 7. Stability regions of phase-locked solutions of system (15) with a uniform distribution (6): green regions correspond to stable in-phase solutions only, gray regions correspond to stable anti-phase solutions only, and yellow indicates the region where both types of phase-locked solutions coexist and are stable. (a) $\rho = 0.0001$, (b) $\rho = 0.5$, (c) $\rho = 1.5$, and (d) $\rho = 2$.

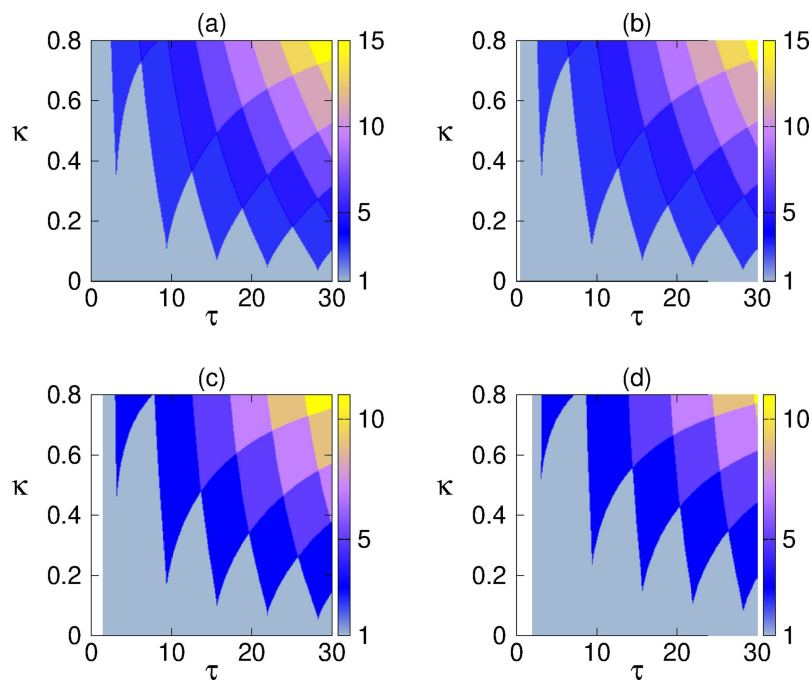


FIG. 8. Total number of stable in-phase solutions of the system (15) with a uniform distribution (6). The color bar corresponds to the number of possible frequencies at each point. (a) $\rho = 0.0001$, (b) $\rho = 0.5$, (c) $\rho = 1.5$, and (d) $\rho = 2$.

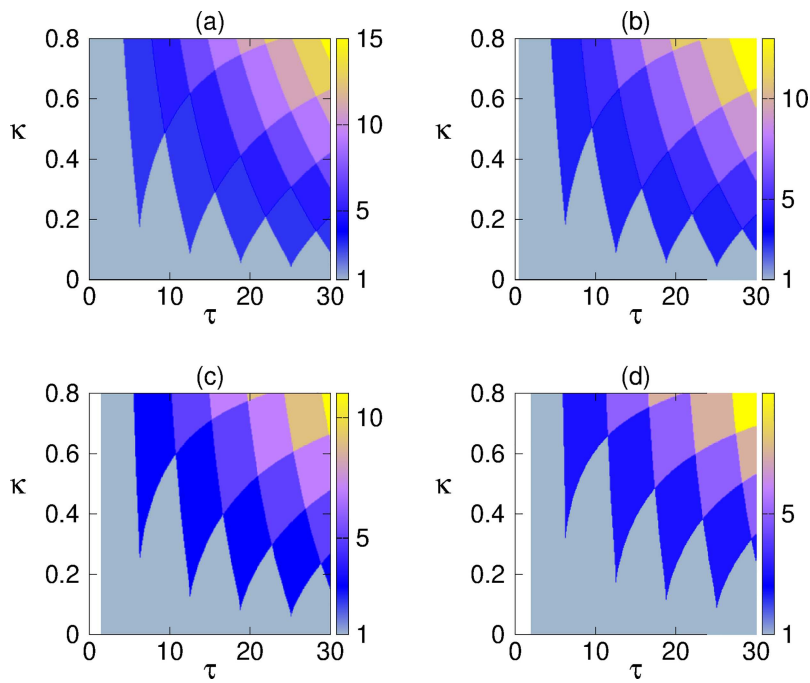


FIG. 9. Total number of stable anti-phase solutions of the system (15) with a uniform distribution (6). The color bar corresponds to the number of possible frequencies at each point. (a) $\rho = 0.0001$, (b) $\rho = 0.5$, (c) $\rho = 1.5$, and (d) $\rho = 2$.

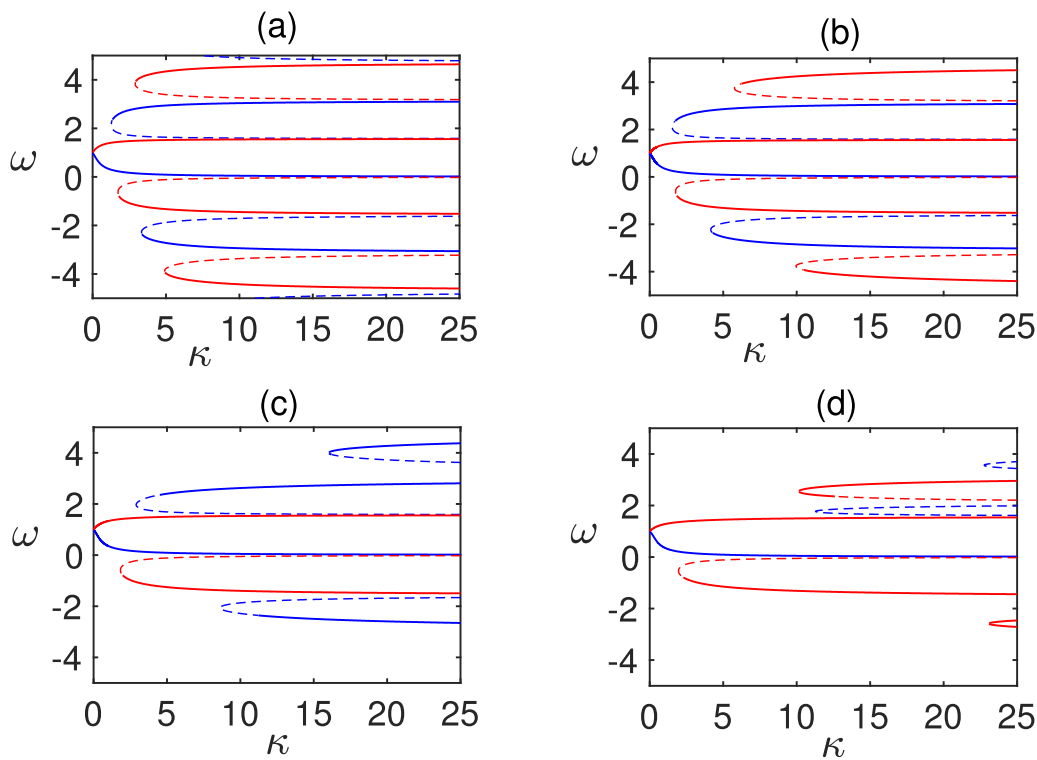


FIG. 10. Branches of phase-locked solutions of (15) with a uniform distribution (6) with $\tau = 2$ and different distribution widths. Solid lines denote stable branches, and dashed lines denote unstable branches. Blue indicates in-phase solutions and red anti-phase solutions. (a) $\rho = 0.0001$, (b) $\rho = 0.5$, (c) $\rho = 1$, and (d) $\rho = 1.5$.

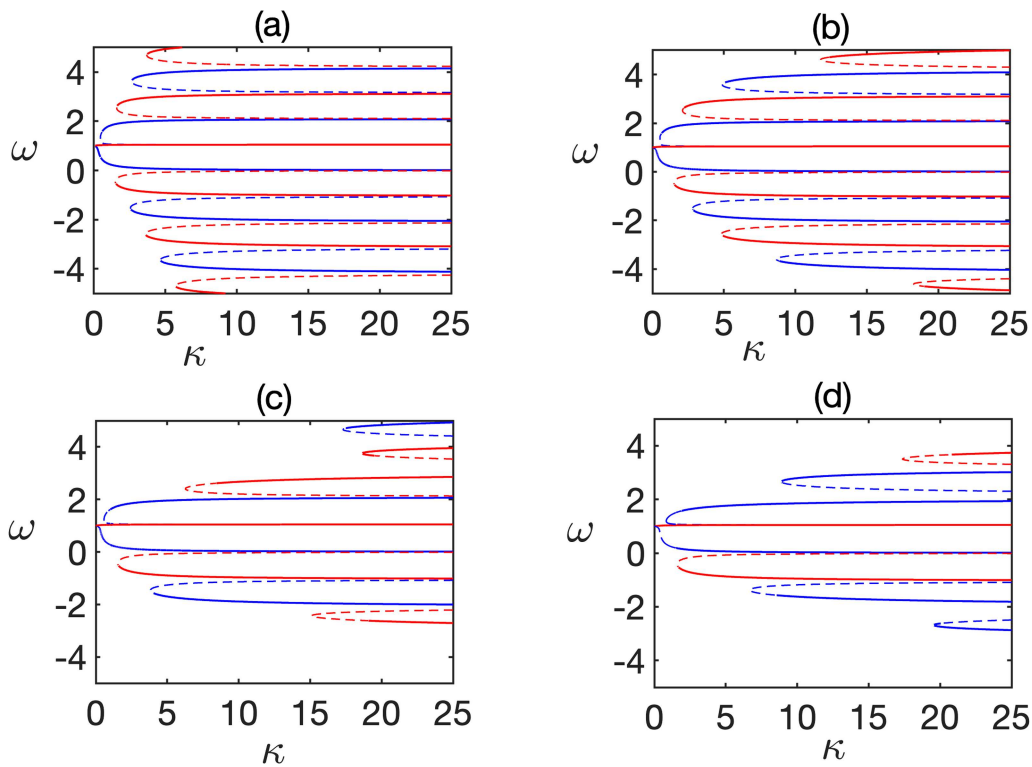


FIG. 11. Branches of phase-locked solutions of (15) with a uniform distribution (6) with $\tau = 3$ and different distribution widths. Solid lines denote stable branches, and dashed lines denote unstable branches. Blue indicates in-phase solutions and red anti-phase solutions. (a) $\rho = 0.0001$, (b) $\rho = 0.5$, (c) $\rho = 1$, and (d) $\rho = 1.5$.

which gives similar conditions $\kappa \cos(\omega\tau_m) > 0$ and $\kappa \cos(\omega\tau_m) < 0$ for stability of the in-phase and anti-phase solutions, respectively, where now the mean time delay τ_m has the form $\tau_m = 2/\gamma$. Figure 6 illustrates regions of stability of different solutions, and similarly to the case of a weak gamma distribution, we observe alternating regions where only in-phase or anti-phase solutions are stable for smaller values for κ , whereas for sufficiently high κ , there is multistability. We note that for the same values of γ , multistability occurs for smaller values of the coupling strength, and for the same value of κ , stability regions are wider in terms of γ values.

Remark. A straightforward manipulation of the characteristic equation (10) shows that for a gamma distribution with a general integer value of parameter p , stability conditions for the in-phase and anti-phase solutions are given, respectively, as $\kappa \cos(\omega\tau_m) > 0$ and $\kappa \cos(\omega\tau_m) < 0$, where the mean time delay of that distribution is $\tau_m = p/\gamma$. From the explicit form of the characteristic equation (10), it follows that similarly to the case of the uniform distribution, for the gamma distribution, the phase-locked solutions can lose/gain stability only through a steady-state bifurcation.

III. DELAY DISTRIBUTION OUTSIDE THE COUPLING FUNCTION

In this section, we consider an alternative way to implement delay-distributed coupling, where the distribution is taken

outside the sine function, which gives the following system of equations:

$$\begin{aligned} \dot{\theta}_1(t) &= 1 + \kappa \int_0^\infty g(s) \sin(\theta_2(t-s) - \theta_1(t)) ds, \\ \dot{\theta}_2(t) &= 1 + \kappa \int_0^\infty g(s) \sin(\theta_1(t-s) - \theta_2(t)) ds, \end{aligned} \tag{15}$$

where θ_1, θ_2 are the phases of the oscillators, κ is the coupling strength, and $g(\cdot)$ is the kernel of the delay distribution, which is again assumed to be positive-definite and normalized to unity. The in-phase/anti-phase frequencies can be found by solving an equation

$$\omega = 1 \mp \kappa \int_0^\infty g(s) \sin(\omega s) ds, \tag{16}$$

and this represents a linear growth of phases with the global frequency ω . Linearizing the system (15) near in-phase/anti-phase solutions yields

$$\begin{aligned} \dot{\phi}_1(t) &= a \left(\pm \int_0^\infty G(s) \phi_2(t-s) ds \mp \phi_1(t) \right), \\ \dot{\phi}_2(t) &= a \left(\pm \int_0^\infty G(s) \phi_1(t-s) ds \mp \phi_2(t) \right), \end{aligned} \tag{17}$$

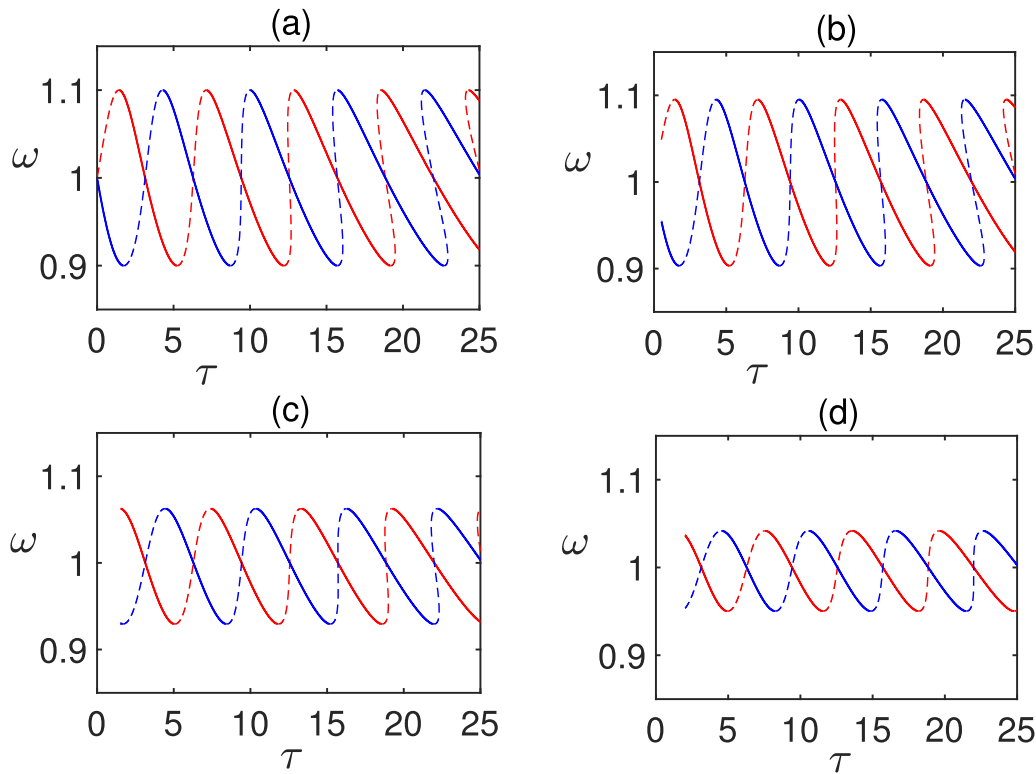


FIG. 12. Branches of phase-locked solutions of (15) with a uniform distribution (6) and $\kappa = 0.1$ for different distribution widths. Solid lines denote stable branches, and dashed lines denote unstable branches. Blue indicates in-phase solutions and red anti-phase solutions. (a) $\rho = 0.0001$, (b) $\rho = 0.5$, (c) $\rho = 1.5$, and (d) $\rho = 2$.

where $a = \kappa \int_0^\infty g(s) \cos(\omega s) ds$ and $G(s) = \frac{1}{a} \kappa g(s) \cos(\omega s)$. The corresponding characteristic equation for the eigenvalues λ is

$$\left[\lambda \pm \kappa \int_0^\infty g(s) \cos(\omega s) ds \right]^2 - \kappa^2 \left[\int_0^\infty g(s) \cos(\omega s) ds \{\mathcal{L}G\}(\lambda) \right]^2 = 0, \tag{18}$$

where $\{\mathcal{L}G\}(\lambda)$ is the Laplace transform of the function $G(s)$.

A. Uniform distribution

In the case of the uniformly distributed kernel (6), we have

$$a = \kappa \int_0^\infty g(s) \cos(\omega s) ds = \frac{\kappa}{2\rho\omega} \cos(\omega\tau) \sin(\omega\rho) \tag{19}$$

and

$$G(s) = \frac{\kappa g(s) \cos(\omega s)}{\frac{\kappa}{2\rho\omega} [\sin(\omega(\tau + \rho)) - \sin(\omega(\tau - \rho))]} = \begin{cases} \frac{\omega \cos(\omega s)}{\sin(\omega(\tau + \rho)) - \sin(\omega(\tau - \rho))}, & \tau - \rho \leq s \leq \tau + \rho, \\ 0 & \text{otherwise.} \end{cases}$$

Hence, the Laplace transform $\{\mathcal{L}G\}(\lambda)$ can be found as

$$\{\mathcal{L}G\}(\lambda) = \frac{\kappa e^{-\lambda\tau}}{2\rho a(\lambda^2 + \omega^2)} \left[-\lambda (e^{-\lambda\rho} \cos(\omega(\tau + \rho)) - e^{\lambda\rho} \cos(\omega(\tau - \rho))) + \omega (e^{-\lambda\rho} \sin(\omega(\tau + \rho)) - e^{\lambda\rho} \sin(\omega(\tau - \rho))) \right]. \tag{20}$$

Rewriting the linearized system with the uniformly distributed kernel with $\phi = (\phi_1, \phi_2)$ yields

$$\dot{\phi}(t) = L_0 \phi(t) + \frac{1}{2\rho} \int_{-(\tau+\rho)}^{-(\tau-\rho)} M \phi(t+s) ds, \tag{21}$$

where

$$L_0 = \begin{pmatrix} \mp a & 0 \\ 0 & \mp a \end{pmatrix}, \quad M = \begin{pmatrix} 0 & \pm a \\ \pm a & 0 \end{pmatrix}$$

for the in-phase/anti-phase solutions, respectively, and we use this form to investigate the stability regions of the in-/anti-phase solutions numerically.

In Fig. 7, stable in- and anti-phase solutions are alternating for small coupling strengths κ , and increase in the coupling strength results in multistability. In contrast to Sec. II, where the delay distribution was included inside the coupling function, in this case, increasing the width of the delay distribution ρ increases the

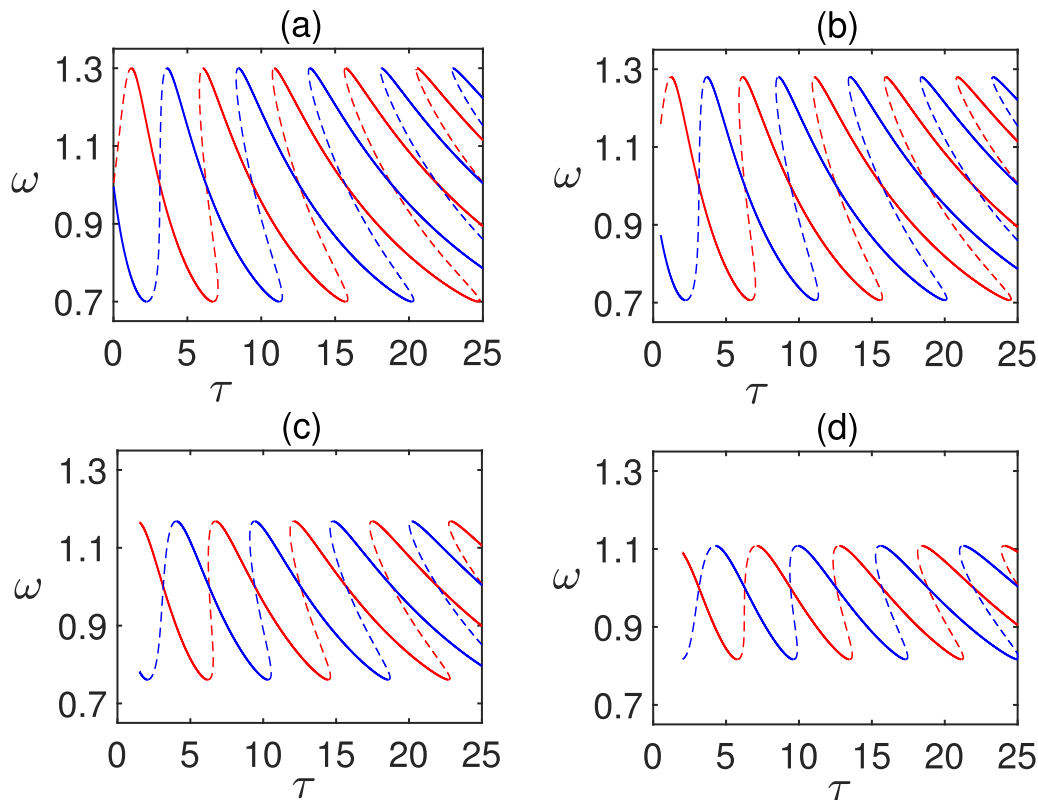


FIG. 13. Branches of phase-locked solutions of (15) with a uniform distribution (6) and $\kappa = 0.3$ for different distribution widths. Solid lines denote stable branches, and dashed lines denote unstable branches. Blue indicates in-phase solutions and red anti-phase solutions. (a) $\rho = 0.0001$, (b) $\rho = 0.5$, (c) $\rho = 1.5$, and (d) $\rho = 2$.

regions where stable in-/anti-phase solutions occur. In particular, we observe an increase in the range of values of the coupling strength κ where only one type of stable phase-locked solutions occurs.

To obtain a better insight into the structure of multistable behavior, in Figs. 8 and 9, we have computed the total number of stable in- and anti-phase solutions for the same parameter range, as demonstrated in Fig. 7. It can be observed that increasing the width of distribution ρ drives a decrease in the number of stable in-phase solutions and a slight increase in the number of stable anti-phase solutions.

Figures 10 and 11 show branches of stable and unstable in-/anti-phase solutions for different values of the time delay τ and increasing width of the distribution ρ . We can see that for small distribution widths ($\rho = 0.0001$, $\rho = 0.5$), in-phase and anti-phase states alternate, but as ρ is increased further, with $\tau = 2$, it leads to the loss of almost all stable in-phase solutions as shown in Fig. 10(d). In contrast, for larger τ , stable in-phase branches persist even for rather large widths ρ , as is observed in Fig. 11(d). In both of these figures, weaker coupling strength κ and larger distribution width ρ are associated with a reduction in the number of possible stable and unstable branches, together with a change in stability of in- and anti-phase branches.

As can be seen in Figs. 12 and 13, there are multiple solutions for the collective frequency ω for sufficiently large values of the mean time delay τ . While only a single frequency is stable for smaller τ , as the value of τ increases, this leads to the emergence of several simultaneously stable frequencies. Comparison of these two figures highlights that the overlapping multistable region increases with increasing value of the coupling strength κ . At the same time, as we increase the width ρ , i.e., make the distribution broader, this narrows the possible range of locking frequencies. In all cases, the change in stability of individual branches occurs as a result of the steady-state bifurcation.

B. Gamma distribution

In this section, we consider the delay kernel given by a gamma distribution of order $p = 1$ so that $g(s) = \gamma e^{-\gamma s}$; hence,

$$a = \kappa \int_0^\infty \gamma e^{-\gamma s} \cos(\omega s) ds, \quad G(s) = \frac{\gamma e^{-\gamma s} \cos(\omega s)}{\int_0^\infty \gamma e^{-\gamma s} \cos(\omega s) ds}. \quad (22)$$

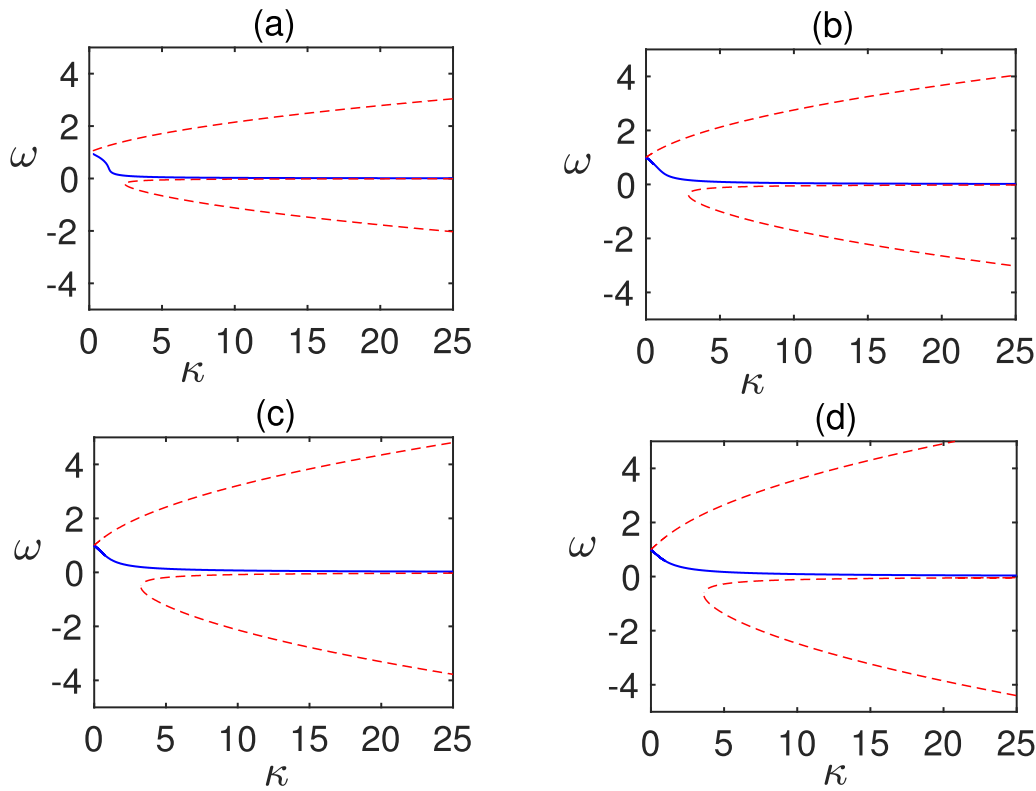


FIG. 14. Branches of phase locked solutions of (15) with a weak ($p = 1$) gamma distribution (9). Solid lines denote stable branches, and dashed lines denote unstable branches. Blue corresponds to in-phase solutions, and red corresponds to anti-phase solutions. (a) $\gamma = 0.25$, (b) $\gamma = 0.5$, (c) $\gamma = 0.75$, and (d) $\gamma = 1$.

We again can use the linear chain trick⁵³ to rewrite the system (17) as a system of ODEs. Introducing new variables

$$\begin{aligned}
 \phi_3(t) &= \frac{1}{b} \int_0^\infty \gamma e^{-\gamma s} \cos(\omega s) \phi_2(t-s) ds, \\
 \phi_4(t) &= \frac{1}{b} \int_0^\infty \omega e^{-\gamma s} \sin(\omega s) \phi_2(t-s) ds, \\
 \phi_5(t) &= \frac{1}{b} \int_0^\infty \gamma e^{-\gamma s} \cos(\omega s) \phi_1(t-s) ds, \\
 \phi_6(t) &= \frac{1}{b} \int_0^\infty \omega e^{-\gamma s} \sin(\omega s) \phi_1(t-s) ds,
 \end{aligned}
 \tag{23}$$

where $b = \int_0^\infty \gamma e^{-\gamma s} \cos(\omega s) ds$, we obtain the following system:

$$\begin{aligned}
 \dot{\phi}_1(t) &= a(\pm\phi_3(t) - \phi_1(t)), \\
 \dot{\phi}_2(t) &= a(\pm\phi_5(t) - \phi_2(t)), \\
 \dot{\phi}_3(t) &= \frac{\gamma}{b} \phi_2(t) - \gamma \phi_3(t) - \gamma \phi_4(t), \\
 \dot{\phi}_4(t) &= -\gamma \phi_4(t) + \frac{\omega^2}{\gamma^2} \phi_3(t),
 \end{aligned}
 \tag{24}$$

$$\dot{\phi}_5(t) = \frac{\gamma}{b} \phi_1(t) - \gamma \phi_5(t) - \gamma \phi_6(t),$$

$$\dot{\phi}_6(t) = -\gamma \phi_6(t) + \frac{\omega^2}{\gamma^2} \phi_5(t).$$

Now, evaluating b gives

$$b = \int_0^\infty \gamma e^{-\gamma s} \cos(\omega s) ds = \frac{\gamma^2}{\gamma^2 + \omega^2},$$

and $a = \kappa b$. The characteristic equation for eigenvalues λ in the case of in-/anti-phase states becomes

$$\begin{aligned}
 &[\lambda(\gamma^2 + \omega^2)(\omega^2 + (\lambda + \gamma)^2) \pm \kappa \gamma^2(\omega^2 + (\lambda + \gamma)^2) + \kappa \gamma^2] \\
 &\times [\lambda(\gamma^2 + \omega^2)(\omega^2 + (\lambda + \gamma)^2) \pm \kappa \gamma^2(\omega^2 + (\lambda + \gamma)^2) - \kappa \gamma^2] \\
 &= 0.
 \end{aligned}
 \tag{25}$$

Figure 14 shows that in the case of a weak gamma distributed kernel, only in-phase solutions are stable, and all anti-phase solutions are unstable independently of the coupling strength κ and the values of γ , which is completely different from the case of the same distribution kernel considered in Sec. II.

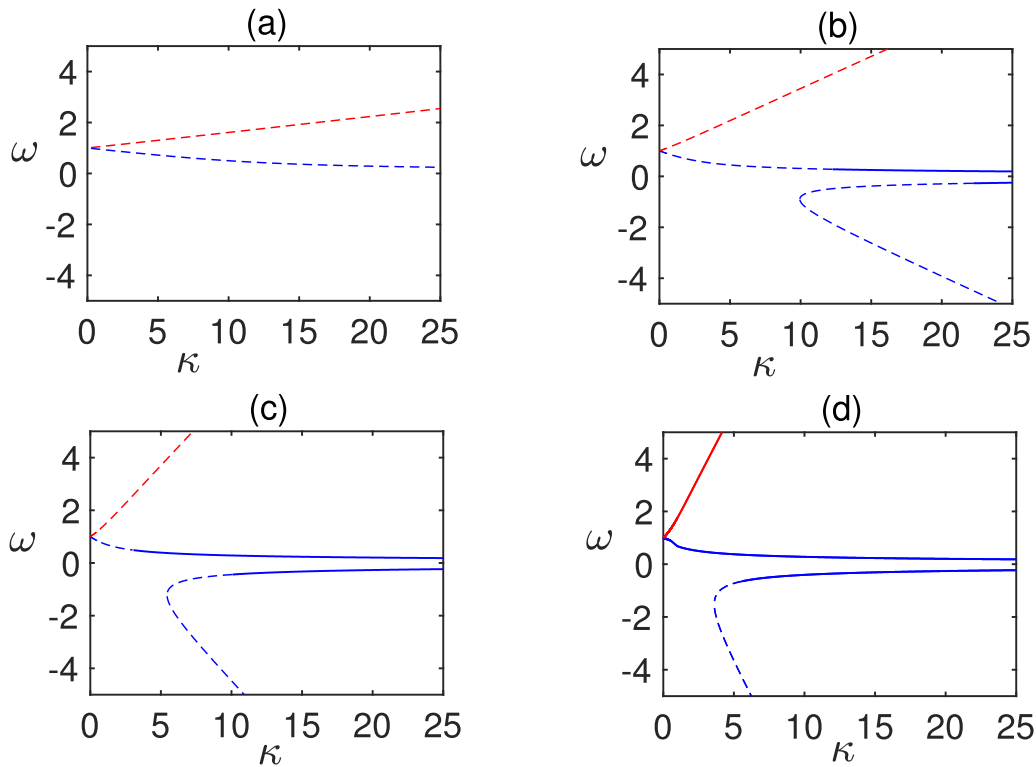


FIG. 15. Branches of phase locked solutions of (15) with a strong ($p = 2$) gamma distribution (9). Solid lines denote stable branches, and dashed lines denote unstable branches. Blue corresponds to in-phase solutions, and red corresponds to anti-phase solutions. (a) $\gamma = 0.25$, (b) $\gamma = 0.5$, (c) $\gamma = 0.75$, and (d) $\gamma = 1$.

Similarly, the system (17) with a strong gamma distributed kernel ($p = 2$) becomes

$$\begin{aligned}
 \dot{\phi}_1(t) &= a(\pm\phi_5(t) - \phi_1(t)), \\
 \dot{\phi}_2(t) &= a(\pm\phi_9(t) - \phi_2(t)), \\
 \dot{\phi}_3(t) &= \frac{\gamma}{b}\phi_2(t) - \gamma\phi_3(t) - \gamma\phi_4(t), \\
 \dot{\phi}_4(t) &= -\gamma\phi_4(t) + \frac{\omega^2}{\gamma^2}\phi_3(t), \\
 \dot{\phi}_5(t) &= \gamma\phi_3(t) - \gamma\phi_5(t) - \gamma^2\phi_6(t), \\
 \dot{\phi}_6(t) &= \gamma\phi_4(t) - \gamma\phi_6(t) + \frac{\omega^2}{\gamma^2}\phi_5(t), \\
 \dot{\phi}_7(t) &= \frac{\gamma}{b}\phi_1(t) - \gamma\phi_7(t) - \gamma\phi_8(t), \\
 \dot{\phi}_8(t) &= -\gamma\phi_8(t) + \frac{\omega^2}{\gamma^2}\phi_7(t), \\
 \dot{\phi}_9(t) &= \gamma\phi_7(t) - \gamma\phi_9(t) - \gamma^2\phi_{10}(t), \\
 \dot{\phi}_{10}(t) &= \gamma\phi_8(t) - \gamma\phi_{10}(t) + \frac{\omega^2}{\gamma^2}\phi_9(t),
 \end{aligned}
 \tag{26}$$

where

$$a = \frac{\kappa\gamma^2(\gamma^2 - \omega^2)}{(\gamma^2 + \omega^2)^2}, \quad b = \frac{\gamma^2(\gamma^2 - \omega^2)}{(\gamma^2 + \omega^2)^2}.$$

Its characteristic equation has the form

$$\begin{aligned}
 & \left[\lambda(\gamma^2 + \omega^2)^2 \pm \kappa\gamma^2(\gamma^2 - \omega^2) + \kappa\gamma^2(\gamma^2 - \omega^2)\{\mathcal{L}G\}(\lambda) \right] \\
 & \times \left[\lambda(\gamma^2 + \omega^2)^2 \pm \kappa\gamma^2(\gamma^2 - \omega^2) - \kappa\gamma^2(\gamma^2 - \omega^2)\{\mathcal{L}G\}(\lambda) \right] \\
 & = 0,
 \end{aligned}
 \tag{27}$$

where

$$\{\mathcal{L}G\}(\lambda) = -\frac{(\gamma^2 + \omega^2)^2}{\gamma^2 - \omega^2} \frac{\omega^2 - (\lambda + \gamma)^2}{(\omega^2 + (\lambda + \gamma)^2)^2}.$$

The branches of stable and unstable in- and anti-phase solutions in the case of a strong gamma distribution are plotted in Fig. 15 for increasing values of γ . For small values of γ , all branches of phase-locked solutions are unstable for any values of κ , but as γ is increased, for large enough values of the coupling strength κ , in Fig. 15(b), there appear branches of stable in-phase solutions. A further increase in γ allows for the stable in-phase solutions to exist for a weaker coupling κ , and for very large γ , an anti-phase solution also gets stabilized for a sufficiently weak coupling strength and large enough locking frequency ω .

IV. DISCUSSION

In this paper, we have analyzed the effects of the delay distribution on the existence and stability of phase-locked solutions for two mutually coupled Kuramoto oscillators. In particular, we have considered two cases of how the delay distribution enters the system. In the first case, the delay distribution was included inside the coupling function, and the system was analyzed for a general distribution, as well as uniform and gamma distributions to find branches of stable and unstable phase-locked solutions, where both oscillators have the same common frequency and, possibly, a constant phase shift. Stability regions for both in- and anti-phase solutions as well as multistability regions were numerically computed for uniform and gamma distributions in terms of the mean time delay, distribution width, coupling strength, and gamma distribution parameters. In the case of a uniform distribution, the solutions alternate between stable in- and anti-phase states, with regions of stability being larger for smaller values of the mean time delay τ . For large values of τ and strong coupling, there are large regions of multistability, where both types of phase-locked solutions coexist and are stable. The width of the distribution ρ does not appear to influence stability properties of the solutions, though it sets the lower bound on the mean time delay, for which phase-locked solutions exist. In the case of the gamma distribution, for small values of parameter γ , which corresponds to larger values of the mean time delay, one again observes switches between regions, where only in-phase or anti-phase solutions are stable, and the size of these regions itself grows with γ , while higher values of the coupling strength are associated with multistability.

To understand the effect of different ways, in which a delayed distribution can be introduced into the system, we have also considered the case of two mutually coupled Kuramoto oscillators, where the distribution is taken outside of the coupling function. We have analytically calculated phase-locking frequencies in terms of the general distribution kernel and the coupling strength. As in the first case, we have concentrated on analyzing the stability of phase-locked states for uniform and gamma distributions. In this case, increasing the width of the uniform distribution increases the size of parameter regions where only one of the phase-locked solutions is stable. The solutions still alternate between stable in- and anti-phase states for weaker coupling strengths, but an increase in the distribution width ρ decreases the range of values of κ where both solutions coexist. For the same values of the mean time delay τ , a broader distribution changes the structure of phase-locked solutions in terms of reducing the number of stable in-phase branches, while increasing the number of stable anti-phase solutions. For a weak gamma distribution in this case, there are no stable anti-phase solutions for any values of the coupling strength κ even for high values of γ . With a strong gamma-distributed kernel, for smaller values of γ , all phase-locked solutions are unstable, while an increase in γ allows for coexistence of stable and unstable in-phase solutions with unstable anti-phase solutions. For larger values of γ and a range of small values of the coupling strength κ , stable phase-locked solutions can coexist with other branches of the same type of solutions or with stable anti-phase solutions.

The results indicate that the delay distribution inside the coupling function does not appear to alter stability of phase-locked solutions in a system of coupled Kuramoto oscillators, only affecting

when they exist. However, having the distribution outside the coupling function does play a role in terms of both existence, as well as stability of phase-locked solutions. Moreover, not only the mean time delay, but also the type of distribution kernel is an important factor in determining when/whether such solutions exist and are stable. So far, we have concentrated on the system of only two coupled Kuramoto oscillators, and one possible extension of this work would be the analysis of an interplay between various network motifs/topologies and delay distributions, as was done for the case of discrete delays in Ref. 50.

ACKNOWLEDGMENTS

The authors would like to thank Otti D’Huys for valuable comments and suggestions in the early stages of this research. A.R. acknowledges funding for her Ph.D. studies from the Engineering and Physical Sciences Research Council (EPSRC) through iCASE Award No. EP/N509784/1.

APPENDIX: DERIVATION OF A LINEARIZED MODEL

To linearize the system (2), we introduce a small perturbation around the in-phase solution as follows:

$$\begin{aligned}\theta_1(t) &= \omega t + \epsilon \phi_1(t), \\ \theta_2(t) &= \omega t + \epsilon \phi_2(t),\end{aligned}$$

where $0 < |\epsilon| \ll 1$. Substituting this into the model (2) yields

$$\begin{aligned}\omega + \epsilon \dot{\phi}_1(t) &= 1 + \kappa \sin \\ &\times \left[\int_0^\infty g(s)(\omega(t-s) + \epsilon \phi_2(t-s)) ds - \omega t - \epsilon \phi_1(t) \right], \\ \omega + \epsilon \dot{\phi}_2(t) &= 1 + \kappa \sin \\ &\times \left[\int_0^\infty g(s)(\omega(t-s) + \epsilon \phi_1(t-s)) ds - \omega t - \epsilon \phi_2(t) \right].\end{aligned}$$

Taylor’s expansion for $|\epsilon| \ll 1$ leads to the linearized system for the in-phase solution as

$$\begin{aligned}\dot{\phi}_1(t) &= \kappa \cos \left[\omega \int_0^\infty sg(s) ds \right] \left[\int_0^\infty g(s) \phi_2(t-s) ds - \phi_1(t) \right], \\ \dot{\phi}_2(t) &= \kappa \cos \left[\omega \int_0^\infty sg(s) ds \right] \left[\int_0^\infty g(s) \phi_1(t-s) ds - \phi_2(t) \right].\end{aligned}\tag{A1}$$

The system (A1) can be rewritten in the matrix form

$$\begin{aligned}\frac{d}{dt} \begin{pmatrix} \phi_1 \\ \phi_2 \end{pmatrix} &= \begin{pmatrix} -\kappa \cos(\omega\tau_m) & 0 \\ 0 & -\kappa \cos(\omega\tau_m) \end{pmatrix} \begin{pmatrix} \phi_1 \\ \phi_2 \end{pmatrix} \\ &+ \begin{pmatrix} 0 & \kappa \cos(\omega\tau_m) \\ \kappa \cos(\omega\tau_m) & 0 \end{pmatrix} \begin{pmatrix} \int_0^\infty g(s) \phi_2(t-s) ds \\ \int_0^\infty g(s) \phi_1(t-s) ds \end{pmatrix},\end{aligned}$$

where $\tau_m = \int_0^\infty sg(s)ds$ is the mean time delay. Letting

$$L_0 = \begin{pmatrix} -\kappa \cos(\omega\tau_m) & 0 \\ 0 & -\kappa \cos(\omega\tau_m) \end{pmatrix}$$

and

$$M = \begin{pmatrix} 0 & \kappa \cos(\omega\tau_m) \\ \kappa \cos(\omega\tau_m) & 0 \end{pmatrix},$$

one recovers the linearized equation (8) used for numerical computations of eigenvalues. Similar calculations can be performed for an anti-phase solution.

DATA AVAILABILITY

The data that support the findings of this study are available within the article.

REFERENCES

- ¹S. Strogatz, "Exploring complex networks," *Nature* **410**, 268–276 (2001).
- ²S. Strogatz, "From Kuramoto to Crawford: Exploring the onset of synchronization in populations of coupled oscillators," *Physica D* **143**, 1–20 (2000).
- ³M. Rohden, A. Sorge, M. Timme, and D. Witthaut, "Self-organized synchronization in decentralized power grids," *Phys. Rev. Lett.* **109**, 064101 (2012).
- ⁴T. Banerjee, D. Biswas, D. Ghosh, E. Schöll, and A. Zakharova, "Networks of coupled oscillators: From phase to amplitude chimeras," *Chaos* **28**, 113124 (2018).
- ⁵H. Fukuda, N. Nakamichi, M. Hisatsune, H. Murase, and T. Mizuno, "Synchronization of plant circadian oscillators with a phase delay effect of the vein network," *Phys. Rev. Lett.* **99**, 098102 (2007).
- ⁶L. Glass, "Synchronization and rhythmic processes in physiology," *Nature* **410**, 277–284 (2001).
- ⁷S. Boccaletti, V. Latora, Y. Moreno, M. Chavez, and D.-U. Hwang, "Complex networks: Structure and dynamics," *Phys. Rep.* **424**, 175–308 (2006).
- ⁸A. Pikovsky, M. Rosenblum, and J. Kurths, *Synchronization: A Universal Concept in Nonlinear Sciences* (Cambridge University Press, 2003), Vol. 12.
- ⁹S. Shahal, A. Wurzberg, I. Sibony, H. Duadi, E. Shniderman, D. Weymouth, N. Davidson, and M. Fridman, "Synchronization of complex human networks," *Nat. Commun.* **11**, 3854 (2020).
- ¹⁰T. Chouzouris, I. Omelchenko, A. Zakharova, J. Hlinka, P. Jiruska, and E. Schöll, "Chimera states in brain networks: Empirical neural vs. modular fractal connectivity," *Phys. Rep.* **424**, 175–308 (2006).
- ¹¹J. Hindes, K. Szwaykowska, and I. Schwartz, "Hybrid dynamics in delay-coupled swarms with motherhood networks," *Phys. Rev. E* **94**, 032306 (2016).
- ¹²A. Winfree, "Biological rhythms and the behavior of populations of coupled oscillators," *J. Theor. Biol.* **16**, 15–42 (1967).
- ¹³Y. Kuramoto, "Self-entrainment of a population of coupled non-linear oscillators," in *International Symposium on Mathematical Problems in Theoretical Physics* (Springer, 1975), Vol. 39, pp. 420–422.
- ¹⁴R. Berner, S. Vock, E. Schöll, and S. Yanchuk, "Desynchronization transitions in adaptive networks," *Phys. Rev. Lett.* **126**, 028301 (2021).
- ¹⁵C. Zhou and J. Kurths, "Dynamical weights and enhanced synchronization in adaptive complex networks," *Phys. Rev. Lett.* **96**, 164102 (2006).
- ¹⁶M. Aguiar and A. Dias, "Synchronization and equitable partitions in weighted networks," *Chaos* **28**, 073105 (2018).
- ¹⁷Y. Wu, Y. Shang, M. Chen, C. Zhou, and J. Kurths, "Synchronization in small-world networks," *Chaos* **18**, 037111 (2008).
- ¹⁸Y. Kuramoto and D. Battogtokh, "Coexistence of coherence and incoherence in nonlocally coupled phase oscillators," *Nonlinear Phenom. Complex Syst.* **5**, 380–385 (2002).
- ¹⁹D. M. Abrams and S. H. Strogatz, "Chimera states for coupled oscillators," *Phys. Rev. Lett.* **93**, 174102 (2004).
- ²⁰E. Schöll, "Synchronization patterns and chimera states in complex networks: Interplay of topology and dynamics," *Eur. Phys. J.: Spec. Top.* **225**, 891–919 (2016).
- ²¹V. Nicosia, M. Valencia, M. Chavez, A. Diaz-Guilera, and V. Latora, "Remote synchronization reveals network symmetries and functional modules," *Phys. Rev. Lett.* **110**, 174102 (2013).
- ²²J. Sawicki, I. Omelchenko, A. Zakharova, and E. Schöll, "Delay controls chimera relay synchronization in multiplex networks," *Phys. Rev. E* **98**, 062224 (2018).
- ²³F. Sorrentino, L. Pecora, A. Hagerstrom, T. Murphy, and R. Roy, "Complete characterization of the stability of cluster synchronization in complex dynamical networks," *Sci. Adv.* **2**, e1501737 (2016).
- ²⁴V. Belykh, G. Osipov, V. Petrov, J. Suykens, and J. Vandewalle, "Cluster synchronization in oscillatory networks," *Chaos* **18**, 037106 (2008).
- ²⁵A. Groth and M. Ghil, "Synchronization of world economic activity," *Chaos* **27**, 127002 (2017).
- ²⁶Y. Ikeda, H. Aoyama, and H. Yoshikawa, "Synchronization and the coupled oscillator model in international business cycles," RIETI Discussion Papers No. 3-E-089, 2013.
- ²⁷F. Atay, *Complex Time-Delay Systems: Theory and Applications* (Springer, 2010).
- ²⁸E. Mallada and A. Tang, "Synchronization of weakly coupled oscillators: Coupling, delay and topology," *J. Phys. A: Math. Theor.* **46**, 505101 (2013).
- ²⁹T. Erneux, J. Javaloyes, M. Wolfrum, and S. Yanchuk, "Introduction to Focus Issue: Time-delay dynamics," *Chaos* **27**, 114201 (2017).
- ³⁰T. Erneux, *Applied Delay Differential Equations* (Springer, 2009).
- ³¹C.-U. Choe, T. Dahms, P. Hövel, and E. Schöll, "Controlling synchrony by delay coupling in networks: From in-phase to splay and cluster states," *Phys. Rev. E* **81**, 025205 (2010).
- ³²D. Dudkowskii, J. Grabski, J. Wojewoda, P. Perlikowski, Y. Maistrenko, and T. Kapitaniak, "Experimental multistable states for small network of coupled pendula," *Nat. Sci. Rep.* **6**, 29833 (2016).
- ³³A. Kashchenko, "Multistability in a system of two coupled oscillators with delayed feedback," *J. Differ. Equ.* **266**, 562–579 (2019).
- ³⁴S. Campbell and Z. Wang, "Phase models and clustering in networks of oscillators with delayed coupling," *Physica D* **363**, 44–55 (2018).
- ³⁵A. Zakharova, I. Schneider, Y. N. Kyrchko, K. B. Blyuss, A. Koseska, B. Fiedler, and E. Schöll, "Time delay control of symmetry-breaking primary and secondary oscillation death," *Europhys. Lett.* **104**, 50004 (2013).
- ³⁶F. Atay, "Distributed delays facilitate amplitude death of coupled oscillators," *Phys. Rev. Lett.* **91**, 094101 (2003).
- ³⁷P. C. Bressloff, S. Coombes, and B. de Souza, "Dynamics of a ring of pulse-coupled oscillators: Group-theoretic approach," *Phys. Rev. Lett.* **79**, 2791 (1997).
- ³⁸Y. N. Kyrchko, K. B. Blyuss, and E. Schöll, "Amplitude death in systems of coupled oscillators with distributed-delay coupling," *Eur. Phys. J. B* **84**, 307–315 (2011).
- ³⁹Y. N. Kyrchko, K. B. Blyuss, and E. Schöll, "Amplitude and phase dynamics in oscillators with distributed-delay coupling," *Philos. Trans. R. Soc. London, Ser. A* **371**, 20120466 (2013).
- ⁴⁰B. Rahman, K. B. Blyuss, and Y. N. Kyrchko, "Aging transition in systems of oscillators with global distributed-delay coupling," *Phys. Rev. E* **96**, 032203 (2017).
- ⁴¹B. Rahman, K. B. Blyuss, and Y. N. Kyrchko, "Dynamics of neural systems with discrete and distributed time delays," *SIAM J. Appl. Dyn. Syst.* **14**, 2069–2095 (2015).
- ⁴²L. Pecora and T. Carroll, "Master stability functions for synchronized coupled systems," *Phys. Rev. Lett.* **80**, 2109 (1998).
- ⁴³T. D. J. Lehnert and E. Schöll, "Cluster and group synchronization in delay-coupled networks," *Phys. Rev. E* **86**, 016202 (2012).
- ⁴⁴V. Flunkert, S. Yanchuk, T. Dahms, and E. Schöll, "Synchronizing distant nodes: A universal classification of networks," *Phys. Rev. Lett.* **105**, 254101 (2010).
- ⁴⁵Y. N. Kyrchko, K. B. Blyuss, and E. Schöll, "Synchronization of networks of oscillators with distributed delay coupling," *Chaos* **24**, 043117 (2014).
- ⁴⁶S. Barbarossa and F. Celano, "Self-organizing sensor networks designed as a population of mutually coupled oscillators," in *IEEE 6th Workshop on Signal Processing Advances in Wireless Communications 2005* (IEEE, 2005), pp. 475–479.

⁴⁷P. Closas, E. Calvo, J. A. Fernandez-Rubio, and A. Pages-Zamora, "Coupling noise effect in self-synchronizing wireless sensor networks," in *IEEE 8th Workshop on Signal Processing Advances in Wireless Communications* (IEEE, 2007), pp. 1–5.

⁴⁸G. Filatrella, A. Nielsen, and N. Pedersen, "Analysis of a power grid using a Kuramoto-like model," *Eur. Phys. J. B* **61**, 485–491 (2008).

⁴⁹H. G. Schuster and P. Wagner, "Mutual entrainment of two limit cycle oscillators with time delayed coupling," *Prog. Theor. Phys.* **81**, 939–945 (1989).

⁵⁰O. D’Huys, R. Vicente, T. Erneux, J. Danckaert, and I. Fischer, "Synchronization properties of network motifs: Influence of coupling delay and symmetry," *Chaos* **18**, 037116 (2008).

⁵¹R. Adler, "A study of locking phenomena in oscillators," *Proc. IEEE* **61**, 1380–1385 (1973).

⁵²D. Breda, S. Maset, and R. Vermiglio, "Pseudospectral approximation of eigenvalues of derivative operators with non-local boundary conditions," *Appl. Num. Math.* **56**, 318–331 (2006).

⁵³N. M. MacDonald, *Time Lags in Biological Systems* (Springer, New York, 1978).